Calcolo (2025) 62:1
https://doi.org/10.1007/s10092-024-00626-9

A fast iterative regularization method for ill-posed problems

Tahar Bechouat[1]

Received: 24 June 2024 / Revised: 14 November 2024 / Accepted: 14 November 2024 /
Published online: 27 November 2024

Abstract
Ill-posed problems manifest in a wide range of scientific and engineering disciplines. The solutions to these problems exhibit a high degree of sensitivity to data perturbations. Regularization methods strive to alleviate the sensitivity exhibited by these solutions. This paper presents a fast iterative scheme for addressing linear ill-posed problems, similar to nonstationary iterated Tikhonov regularization. Both the a-priori and a-posteriori choice rules for regularization parameters are provided, and both rules yield error estimates that are order optimal. In comparison to the nonstationary iterated Tikhonov method, the newly introduced method significantly reduces the required number of iterations to achieve convergence based on an appropriate stopping criterion. The numerical computations provide compelling evidence regarding the efficacy of our new iterative regularization method. Furthermore, the versatility of this method extends to image restorations.

Keywords Ill-posed problems · Iterative regularization · Error estimates · Image deblurring

Mathematics Subject Classification 45B05 · 65R30 · 65J20

1 Introduction

We investigate inverse problems characterized by the equation

$$Ax = y^{\delta}, \tag{1.1}$$

where A represents a bounded linear operator from a Hilbert space X to Hilbert space Y, possessing a non-closed range. The variable y^{δ} represents the measured data, which

✉ Tahar Bechouat
t.bechouat@gmail.com

[1] Department of Mathematics, Faculty of Science and Technology, Mohammed Cherif Messaadia University, 41000 Souk Ahras, Algeria

is susceptible to corruption by an error η, that is, $y^\delta = y + \eta$, where y denotes the exact data. In our analysis, we will make the assumption that a reasonably accurate estimate δ for $\|\eta\|_Y$ is available, indicating that

$$\|\eta\|_Y \leq \delta. \tag{1.2}$$

Given that the operator A has a non-closed range, the Eq. (1.1) is ill-posed, meaning that solutions lack continuity with respect to the data. Consequently, regularization techniques become imperative to acquire meaningful approximations. To delve into the theory of ill-posed problems and explore effective regularization strategies, we refer to the relevant literature [1–3].

In the past few years, there has been a remarkable advancement in iterative methods employed to tackle ill-posed problems. When it comes to handling extensive problems, iterative regularization methods have emerged as a compelling choice compared to alternative approaches. Typically, the iterative scheme for solving Eq. (1.1) can be expressed as follows

$$x_n^\delta = x_{n-1}^\delta + F_n r_{n-1}^\delta, n = 1, 2, \ldots, \tag{1.3}$$

where $r_n^\delta = y^\delta - Ax_n^\delta$ and F_n is an operator mapping from Y to X. The initial guess, denoted as x_0^δ, serves as the starting point, while x_n^δ represents the iterative approximate solution attained at the n-th step.

The classical Landweber iteration (CLI), as an illustration, serves to exemplify the intrinsically sluggish characteristics of iterative regularization methods. The CLI method, outlined in [4], can be defined as (1.3) with $F_n = wA^*$, where A^* represents the adjoint operator of A and w denotes the relaxation parameter. To overcome this drawback in the CLI method, it becomes imperative to introduce acceleration techniques, which are extensively discussed in [5–8]. For example, in [8], Egger and Neubauer considered explored a comprehensive approach involving a preconditioning Landweber iteration within Hilbert scales, where the operator F_n is expressed as $L^{-2s}A^*$, with L representing an operator that satisfies certain specified conditions and $s \in \mathbb{R}$, in [7], Xiong et al. introduced a modified Landweber iteration method (MLI) that draws inspiration from the general fractional regularization method [9]. In this method, the operator F_n in (1.3) is defined as $F_n = \beta(A^*A)^{(\gamma-1)/2}A^*$ for some index $0 \leq \gamma \leq 1$ and $0 < \beta \leq 1/\|A\|^{\gamma+1}$ is the fixed time step length. The body of literature exploring different iteration schemes rooted in the fundamental principles of regularization is extensive, we provide a comprehensive review of the nonstationary iterated Tikhonov method (NSIT) introduced in previous works [10–12]. The NSIT method is defined by Eq. (1.3), where $F_n = (A^*A + \alpha_n I)^{-1}A^*$. Additionally, we highlight the relaxed iterated Tikhonov method (RIT) introduced by Chang et al. [13]. This method, defined in (1.3), employs the operator $F_n = \beta_n(A^*A + \alpha I)^{-1}A^*$, where $\beta_n \in (0, 1)$ represents the relaxation parameter and $\alpha \in (0, 1)$.

A comprehensive discussion on iterative regularization methods can be found in references [6, 15–24] and others. Generally, these iterative methods follow the scheme (1.3), with variations mainly lying in the selection of the initial value x_0^δ and the operator F_n.

So far, the theoretical outcomes of the majority of these studies have been confined to the utilization of a-priori regularization parameter selection principles and considering operator A as compact.

In this paper, we delve into an innovative iterative scheme, derived from an NSIT scheme, and demonstrate that this newly modified approach attains an optimal order when applying the conventional a-priori and a-posteriori parameter selection principles, assuming A is a bounded operator. Our study makes a significant contribution by conducting a comprehensive analysis of the fast Tikhonov iteration scheme. Specifically, we enhance the NSIT method by incorporating an additional factor. Importantly, our method offers the distinct advantage of requiring fewer iterations, and furthermore, we will demonstrate that it achieves a robust error estimate (with exact data) surpassing that of the NSIT method.

In iterative regularization methods, the Morozov discrepancy principle is a widely used stopping criterion. The number of iterations $n^* = n^*(\delta)$ is determined based on this principle, assuming that the support of the exact solution $\widehat{x}$ for Eq. (1.1) (when y^δ is replaced with exact data y) is known. The Morozov discrepancy principle can be determined by considering the following conditions, as described in references [14, 15]:

$$\left\|r_{n^*}^\delta\right\|_Y \leq \tau\delta < \left\|r_n^\delta\right\|_Y, n = 1, 2, \ldots, n^* - 1, \tag{1.4}$$

where $\tau > 1$ is a fixed parameter.

The remaining sections of this paper are structured as follows: Sect. 2 outlines the derivation of the fast iterative regularization method. In Sect. 3, we provide rigorous proof of the error estimates. Section 4 focuses on the convergence analysis of this scheme, utilizing the posterior parameter choice strategy (1.4) for selecting the number of iterated Tikhonov regularization iterations. Moreover, Sect. 5 presents several examples that demonstrate the effectiveness of this regularized method and its applicability to deblurring problems. Finally, in the concluding section, we offer valuable insights and summarize our findings.

2 A fast iteration method

In this section, we delve into the outcomes pertaining to the new iterative scheme put forth in this research. Let A and y^δ be as in ill-posed Eq. (1.1), we define the fast nonstationary iterated Tikhonov scheme (FNSIT) as follows

$$x_0^\delta = 0, x_n^\delta = x_{n-1}^\delta + (F_n^{(1)} + F_n^{(2)})r_{n-1}^\delta, n = 1, 2, \ldots, \tag{2.1}$$

where $F_n^{(1)} = (A^*A + \alpha_n I)^{-1}A^*$, $F_n^{(2)} = \alpha_n(A^*A + \alpha_n I)^{-1}(A^*A + \alpha_n^2 I)^{-1}A^*$ and $\{\alpha_n\}_{n\geq 1}$ is a given sequence of positive numbers.

In scheme (2.1), the operator F_n, denoted as $F_n = F_n^{(1)} + F_n^{(2)}$, is expressed as a composite of two operators. The first operator $F_n^{(1)}$ corresponds to the NSIT scheme (see [10–12]), while the second operator $F_n^{(2)}$ represents an additional factor. Essentially, the FNSIT scheme can be regarded as an augmented NSIT scheme, incorporating an additional acceleration component.

The FNSIT scheme can be interpreted as a preconditioned variant of the Landweber iteration (see [8]), utilizing the preconditioner $(A^*A+\alpha_n I)^{-1}(I+\alpha_n(A^*A+\alpha_n^2 I)^{-1})$.

By employing the exact data, the FNSIT scheme can be expressed as

$$x_0 = 0,\ x_n = x_{n-1} + F_n r_{n-1},\ n = 1, 2, \ldots,$$

where $r_n = y - Ax_n$.

Since $A\widehat{x} = y$, we obtain

$$x_0 = 0,\ x_n = x_{n-1} + F_n(A\widehat{x} - Ax_{n-1}),\ n = 1, 2, \ldots.$$

Thus,

$$e_n = e_{n-1} - F_n A e_{n-1},\ n = 1, 2, \ldots,$$

where $e_n = \widehat{x} - x_n$ is the error after n steps.

Therefore, by induction we have

$$\begin{aligned} e_n &= (I - F_n A)\, e_{n-1} \\ &= (I - F_n A)\,(I - F_{n-1} A)\, e_{n-2} \\ &= \prod_{j=1}^{n} \left(I - F_j A\right) e_0. \end{aligned}$$

Since $e_0 = \widehat{x}$, we obtain

$$e_n = \prod_{j=1}^{n} \left(I - F_j A\right) \widehat{x}.$$

Furthermore, straightforward calculations reveal that

$$\begin{aligned} I - F_j A &= I - \left[(A^*A + \alpha_j I)^{-1} + \alpha_j (A^*A + \alpha_j I)^{-1}(A^*A + \alpha_j^2 I)^{-1}\right] A^*A \\ &= \alpha_j^3 (A^*A + \alpha_j I)^{-1}(A^*A + \alpha_j^2 I)^{-1}. \end{aligned}$$

Thus, the error e_n can be determined by

$$e_n = \prod_{j=1}^{n} h_j(A^*A)\widehat{x}, \tag{2.2}$$

where $h_j(A^*A) = \alpha_j^3 (A^*A + \alpha_j I)^{-1}(A^*A + \alpha_j^2 I)^{-1}$.

In [10], the error e_n in the NSIT scheme with exact data y is given as follows:

$$e_n = \prod_{j=1}^{n} \alpha_j (A^*A + \alpha_j I)^{-1}\widehat{x}. \tag{2.3}$$

Upon examining the results (2.2) and (2.3), we observe that our newly proposed method prominently features the additional factor $F_n^{(2)}$, thereby rendering it faster than the NSIT scheme, which will be demonstrated in the next section.

The approximate solution obtained at the n-th step of the FNSIT method (2.1) is given by

$$\begin{aligned} x_n^\delta &= (I - F_n A)x_{n-1}^\delta + F_n y^\delta, n = 1, 2, \ldots, \\ &= h_n(A^*A)x_{n-1}^\delta + A^*\theta_n(AA^*)y^\delta, n = 1, 2, \ldots, \\ &= h_n(A^*A)x_{n-1}^\delta + \theta_n(A^*A)A^*y^\delta, n = 1, 2, \ldots, \end{aligned}$$

where $\theta_n(\lambda) = (\lambda + \alpha_n)^{-1} + \alpha_n(\lambda + \alpha_n)^{-1}(\lambda + \alpha_n^2)^{-1}$.

Thus, it becomes evident that the computed solution x_n^δ, can be expressed as follows:

$$x_n^\delta = A^* g_n(AA^*)y^\delta = g_n(A^*A)A^*y^\delta, \tag{2.4}$$

where g_n is generated by

$$g_0(\lambda) = 0,\ g_n(\lambda) = h_n(\lambda)g_{n-1}(\lambda) + \theta_n(\lambda).$$

Since $\theta_n(\lambda) = h_n(\lambda)(\lambda/\alpha_n^3 + \left(\alpha_n^2 + \alpha_n\right)/\alpha_n^3)$, then

$$g_n(\lambda) = h_n(\lambda)\left(g_{n-1}(\lambda) + \frac{\lambda}{\alpha_n^3} + \frac{\alpha_n^2 + \alpha_n}{\alpha_n^3}\right).$$

Thus,

$$\begin{aligned} 1 - \lambda g_n(\lambda) &= 1 - \lambda h_n(\lambda)\left(g_{n-1}(\lambda) + \frac{\lambda}{\alpha_n^3} + \frac{\alpha_n^2 + \alpha_n}{\alpha_n^3}\right) \\ &= h_n(\lambda)\left(1 - \lambda g_{n-1}(\lambda)\right). \end{aligned}$$

By utilizing a recurrence relation, we can derive

$$1 - \lambda g_n(\lambda) = \prod_{j=1}^{n} h_j(\lambda).$$

Finally, the function g_n can be expressed as follows

$$g_n(\lambda) = \frac{1 - \prod_{j=1}^{n} h_j(\lambda)}{\lambda}. \tag{2.5}$$

At first glance, the proposed method may appear to have a drawback: each iteration costs twice as much as the NSIT method. However, upon closer examination of its implementation, this perceived drawback dissipates entirely, as exemplified in the following example.

Example 2.1 Assume that A in Eq. (1.1) is a compact operator with the singular system (σ_k, u_k, v_k), i.e., σ_k is a sequence of positive real numbers such that $\sigma_k \to 0$ and $\{u_k\}$, $\{v_k\}$ are orthonormal basis of orthogonal complement to the null space $N(A)$ and the closed range space $\overline{R(A)}$, respectively. It is a well-established fact that any compact operator A, acting between Hilbert spaces X and Y, can be expressed in the form of the singular value expansion

$$Ax = \sum_{k=1}^{rank(A)} \sigma_k \langle x, u_k \rangle_X \, v_k, \; A^* y = \sum_{k=1}^{rank(A)} \sigma_k \langle y, v_k \rangle_Y \, u_k, \tag{2.6}$$

where $rank(A)$ is the dimension of $R(A)$.

Now, assuming $f : \left[0, \|A^*A\|\right] \to \mathbb{R}$ is a bounded function, the functional calculus possesses the following property

$$f(A^*A)x = \sum_{k=1}^{rank(A)} f\left(\sigma_k^2\right) \langle x, u_k \rangle_X \, u_k. \tag{2.7}$$

When applying properties (2.6) and (2.7) to equality (2.4), we get the computed solution x_n^δ by the following relation

$$x_n^\delta = \sum_{k=1}^{rank(A)} g_n\left(\sigma_k^2\right) \left\langle A^* y^\delta, u_k \right\rangle_X u_k = \sum_{k=1}^{rank(A)} \sigma_k g_n\left(\sigma_k^2\right) \left\langle y^\delta, v_k \right\rangle_X u_k.$$

In this case, the approximate solution obtained at the n-th step of the FNSIT method (2.1) is given by

$$x_n^\delta = \sum_{k=1}^{rank(A)} \frac{1}{\sigma_k} \left(1 - \prod_{j=1}^{n} h_j\left(\sigma_k^2\right)\right) \left\langle y^\delta, v_k \right\rangle_X u_k. \tag{2.8}$$

By following the same previous steps, the approximate solution is derived when employing the NSIT method, yielding:

$$x_n^\delta = \sum_{k=1}^{rank(A)} \frac{1}{\sigma_k} \left(1 - \prod_{j=1}^{n} \widetilde{h}_j\left(\sigma_k^2\right)\right) \left\langle y^\delta, v_k \right\rangle_X u_k, \tag{2.9}$$

where $\widetilde{h}_j(\lambda) = \alpha_j(\lambda + \alpha_j)^{-1}$.

From (2.8) and (2.9), the two methods have almost the same formula. But the only difference is in the calculation of the functions h_j and $\widetilde{h}_j$, and this small difference slightly affects the calculations. Therefore, the complexity of calculations for the two methods is almost equal.

3 Error estimate

In this section, we delve into several outcomes pertaining to the FNSIT scheme put forth in this study. To begin with, we establish our assumptions based on the prescribed conditions (refer to [10, 24]) concerning the sequence numbers $\{\alpha_n\}_{n\geq 0}$:

$(C1)$ The sequence $\{\alpha_n\}_{n\geq 1}$ is decreasing with $\lim_{n\to\infty}\alpha_n = 0$.

$(C2)$ There exists a constant $c^{(p)} > 1$ such that

$$\gamma_{n,p} \leq c^{(p)}\gamma_{n-1,p}, \tag{3.1}$$

where $\gamma_{n,p} = \sum_{j=1}^{n} \alpha_j^{-p}$ with $p = 1, 2$.

In the studies [10, 24], condition $C2$ was employed with $p = 1$; nevertheless, in this present study, we adopt condition $C2$ with $p = 2$. For instance, let us consider $\alpha_n = q^n$ $(n \geq 2)$ as a geometric sequence. In this case, conditions $C1$ and $C2$ can be readily verified for $q < 1$ and $c^{(p)} = 1/q + 1$. Consequently, in this particular example, condition $C2$ is satisfied with the identical value of $c^{(p)} = 1/q + 1$.

Considering y as an element belonging to the range of A, we assume that the exact solution $\widehat{x}$ satisfies the smoothness source condition

$$\widehat{x} = \left(A^*A\right)^s u \text{ with } \|u\|_X \leq \rho \text{ and } s > 0. \tag{3.2}$$

In order to assess the error bounds of $\|e_n\|_X$, we proceed by introducing the following Lemma, as referenced in [10].

Lemma 3.1 [10]. *Assuming that the conditions $C1$ and $C2$ are met, and if the source condition (3.2) is satisfied with $0 < s < n$. Then*

$$\sup_{\lambda\geq 0} \lambda^s \prod_{j=1}^{n} \frac{\alpha_j}{\alpha_j + \lambda} \leq c_s \gamma_{n,1}^{-s},$$

where $c_s = \begin{cases} \left(2s(c^{(1)}+1)\right)^s, & 0 < s \leq 1, \\ \left(2s(c^{(1)}+1)^s\right)^s, & 1 < s < n. \end{cases}$

The outcome of the following theorem pertains specifically to the case of exact data y, denoting the noise-free case.

Theorem 3.2 *Assuming that the conditions $C1$ and $C2$ are met, and the smoothness source condition (3.2) hold. Then*

$$\|e_n\|_X \leq \rho c_s \gamma_{n,2}^{-s},$$

where c_s is given in Lemma 3.1 with replace $c^{(1)}$ by $c^{(2)}$.

Proof First, we can represent the error e_n defined in (2.2) by the spectral theorem

$$e_n = \int_0^{\|A^*A\|} f_n(\lambda) dE_\lambda \widehat{x},$$

where $f_n(\lambda) = \prod_{j=1}^n h_j(\lambda)$ and $\{E_\lambda : 0 \leq \lambda \leq \|A^*A\|\}$ is the associated spectral family of the self-adjoint operator A^*A.

By leveraging the source condition (3.2), we obtain

$$e_n = \int_0^{\|A^*A\|} \lambda^s f_n(\lambda) dE_\lambda u.$$

Thus,

$$\begin{aligned} \|e_n\|_X &= \left\| \int_0^{\|A^*A\|} \lambda^s f_n(\lambda) dE_\lambda u \right\|_X \\ &\leq \|u\|_X \sup_{\lambda \geq 0} \left| \lambda^s f_n(\lambda) \right|. \end{aligned}$$

By virtue of Lemma 3.1, we derive

$$\begin{aligned} \|e_n\|_X \leq & \rho \sup_{\lambda \geq 0} \prod_{j=1}^n \frac{\alpha_j}{\alpha_j + \lambda} \sup_{\lambda \geq 0} \lambda^s \prod_{j=1}^n \frac{\alpha_j^2}{\alpha_j^2 + \lambda} \\ \leq & \rho c_s \gamma_{n,2}^{-s}, \end{aligned}$$

where $c_s = \begin{cases} \left(2s(c^{(2)} + 1)\right)^s, & 0 < s \leq 1, \\ \left(2s(c^{(2)} + 1)^s\right)^s, & 1 < s < n. \end{cases}$

The proof of Theorem 3.2 is complete. □

To begin with, the outer inequality in Theorem 3.2 establishes that if the data are exact ($\delta = 0$), it can be deduced that the iterates of the FNSIT method converge to an exact solution $\widehat{x}$ of (1.1) as n approaches infinity. Additionally, Theorem 3.2 implies that our regularized method's error estimate for the optimal solution attained with exact data can be expressed as $O\left(\gamma_{n,2}^{-s}\right)$, while the NSIT method error for the optimal solution obtained with exact data is denoted as $O\left(\gamma_{n,1}^{-s}\right)$ (see [10, 24]). Consequently, the superiority of our scheme in error estimation with exact data compared to the NSIT scheme becomes evident.

In the current analysis, we investigate a case where the precise data y can be replaced by y^δ within the proposed scheme. Prior to delving into the analysis of error estimation, denoted as $e_n^\delta = \widehat{x} - x_n^\delta$, we introduce the following Lemma as a preliminary outcome.

Lemma 3.3 *The function g_n, as defined in (2.5), verifies the conditions:*

$$\sup_{\lambda \geq 0} \lambda g_n(\lambda) \leq 1 \text{ and } \sup_{\lambda \geq 0} g_n(\lambda) \leq 2\gamma_{n,2}.$$

Proof Since $\lambda g_n(\lambda) = 1 - f_n(\lambda)$ and $0 \leq f_n(\lambda) \leq 1$, we obtain

$$\sup_{\lambda \geq 0} \lambda g_n(\lambda) \leq 1.$$

By means of straightforward computation, we obtain

$$\begin{aligned} f_n'(\lambda) &= -\varphi_n(\lambda) f_n(\lambda) \leq 0, \\ f_n''(\lambda) &= f_n(\lambda) \left[\sum_{i=1}^{n} \frac{2\lambda^2 + 2\left(\alpha_i^2 + \alpha_i\right)\lambda + \alpha_i^2\left(\alpha_i^2 + 1\right)}{(\alpha_i + \lambda)^2\left(\alpha_i^2 + \lambda\right)^2} + \varphi_n^2(\lambda) \right] \geq 0, \end{aligned}$$

where $\varphi_n(\lambda) = \sum_{i=1}^{n} \frac{2\lambda + \alpha_i^2 + \alpha_i}{(\alpha_i + \lambda)(\alpha_i^2 + \lambda)}$.

Consequently, since the function f_n' exhibits monotonically non-decreasing behavior over the interval $[0, \infty)$, it follows that f_n is a convex function.

Exploiting the convexity property of f_n over the interval $[0, \infty)$, we derive the following result

$$g_n(\lambda) = \frac{1 - f_n(\lambda)}{\lambda} \leq -f_n'(0) = \sum_{i=1}^{n} \frac{\alpha_i^2 + \alpha_i}{\alpha_i^3}.$$

Thus,

$$g_n(\lambda) \leq \gamma_{n,1} + \gamma_{n,2} \leq 2\gamma_{n,2}.$$

The proof of Lemma 3.3 is complete. □

Theorem 3.4 *Assuming that the conditions C1 and C2 are met, and the smoothness source condition (3.2) hold. Then*

$$\left\| e_n^{\delta} \right\|_X \leq \rho c_s \gamma_{n,2}^{-s} + \sqrt{2\gamma_{n,2}}\delta. \tag{3.3}$$

Proof From (2.4) we obtain

$$\begin{aligned} \left\| x_n - x_n^{\delta} \right\|_X^2 &= \left\langle A^* g_n(AA^*)\left(y - y^{\delta}\right), A^* g_n(AA^*)\left(y - y^{\delta}\right) \right\rangle_X \\ &= \left\langle g_n(AA^*)\eta, AA^* g_n(AA^*)\eta \right\rangle_Y \\ &\leq \left\| g_n(AA^*)\eta \right\|_Y \left\| AA^* g_n(AA^*)\eta \right\|_Y. \end{aligned}$$

Through the application of the spectral theorem and using the result of Lemma 3.3, we get

$$\begin{aligned} \left\| x_n - x_n^{\delta} \right\|_X^2 &\leq \left\| \int_0^{\|AA^*\|} g_n(\lambda) dE_\lambda \eta \right\|_Y \left\| \int_0^{\|AA^*\|} \lambda g_n(\lambda) dE_\lambda \eta \right\|_Y \\ &\leq \sup_{\lambda \geq 0} g_n(\lambda) \sup_{\lambda \geq 0} \lambda g_n(\lambda) \left\| \eta \right\|_Y^2 \\ &\leq 2\gamma_{n,2} \left\| \eta \right\|_Y^2. \end{aligned}$$

Using (1.2), we have

$$\left\|x_n - x_n^\delta\right\|_X \leq \sqrt{2\gamma_{n,2}}\delta.$$

By leveraging the inequality $\left\|e_n^\delta\right\|_X \leq \|e_n\|_X + \left\|x_n - x_n^\delta\right\|_X$ and employing the outcome derived from Theorem 3.2, we are able to deduce the error estimate (3.3).

The proof of Theorem is complete. □

Utilizing Theorem 3.4 enables us to ascertain the achievable level of convergence order within our iterative method. Specifically, if we select $n = n(\delta)$ such that $\lim_{\delta\to 0}\sqrt{\gamma_{n(\delta),2}}\delta = 0$ and $\lim_{\delta\to 0}\gamma_{n(\delta),2} = \infty$, we can conclude that $\lim_{\delta\to 0}\left\|e_{n(\delta)}^\delta\right\|_X = 0$.

For example, if we choose $n = n(\delta)$ such that $\gamma_{n(\delta),2} \approx \delta^{\frac{-2}{2s+1}}$, then

$$\left\|e_{n(\delta)}^\delta\right\|_X \leq \left(\rho c_s + \sqrt{2}\right)\delta^{\frac{2s}{2s+1}}.$$

Suppose we take $\alpha_i = q^i$ to be a geometric sequence. In this case, verifying condition (3.1) is straightforward for $q < 1$, and $c = 1/q + 1$. When we use the a-priori choice from the previous example in Theorem 3.4, we get $\gamma_{n^{FNSIT},2} \approx \delta^{\frac{-2}{2s+1}}$ and $\gamma_{n^{NSIT},1} \approx \delta^{\frac{-2}{2s+1}}$ (refer to [10]), which implies $n^{FNSIT} < n^{NSIT}$. In this cas, we obtain

$$n^{FNSIT} \approx \frac{1}{2}\left(\frac{\ln(1+q)}{\ln(1/q)} + n^{NSIT}\right).$$

For instance, if we set $q = 0.75$, then we have

$$n^{FNSIT} \approx 1 + \frac{n^{NSIT}}{2}. \tag{3.4}$$

The findings illustrate the considerable advancements brought forth by the newly proposed approach when compared to the NSIT method, particularly in two pivotal dimensions. Primarily, the novel method exhibits a resilient error estimation capability (with precise data) for sufficiently small values of $q < 1$. Secondly, as evidenced in the aforementioned example, our method necessitates a reduced number of iterations in contrast to the NSIT method.

In the preceding example, the selection methodology employed for the parameter is commonly denoted as an a-priori strategy, however, an a-posteriori strategy is generally favored. In the subsequent section, we shall employ the Morozov discrepancy principle choice strategy (1.4) to ascertain the convergence rate.

4 A-posteriori regularization parameter choice

In this section, we thoroughly examine the adaptive strategy utilized for the selection of a regularization parameter in the FNSIT scheme. To accomplish this, we delve into the exploration of an a-posteriori regularization parameter choice, which is founded on the Morozov discrepancy principle (1.4).

From (2.4), we have

$$Ax_n^\delta = AA^* g_n(AA^*) y^\delta.$$

Thus,

$$\begin{aligned} r_n^\delta &= \left(I - AA^* g_n(AA^*)\right) y^\delta \\ &= f_n(AA^*) y^\delta. \end{aligned}$$

Therefore,

$$\left\| r_n^\delta \right\|_Y = \left\| \int_0^{\|AA^*\|} f_n(\lambda) dE_\lambda y^\delta \right\|_Y. \tag{4.1}$$

Now, by fixing $\lambda \in [0, \|AA^*\|]$, we ensure that the sequence f_n is monotonically decreasing. As a consequence, the sequence $\left\| r_n^\delta \right\|_Y$ also exhibits a decreasing trend to 0 and

$$\begin{aligned} \left\| r_1^\delta \right\|_Y &= \left\| \int_0^{\|AA^*\|} f_1(\lambda) dE_\lambda y^\delta \right\|_Y \\ &= \sup_{\lambda \in [0, \|AA^*\|]} f_1(\lambda) \left\| y^\delta \right\|_Y \\ &= \left\| y^\delta \right\|_Y. \end{aligned} \tag{4.2}$$

Upon careful examination of equality (4.2), it becomes apparent that the assertions are already valid for the selection of n according to (1.4), given that y^δ fulfills the condition:

$$\left\| y^\delta \right\|_Y > \tau\delta. \tag{4.3}$$

According to condition (4.3), it is evident that there exists a minimum value of $n^* > 1$ that satisfies the condition $\left\| r_{n^*}^\delta \right\|_Y \leq \tau\delta$.

Algorithm 4.1 *Stopping criteria based on Morozov's discrepancy principle.*

Input: $0 < q < 1$, $r_0^\delta = y^\delta$ *and* $\tau > 1$.
for $n = 1, 2, \ldots$ ***do***
1- Compute $\alpha_n = q^n$ *and* x_n^δ *by* $x_n^\delta = x_{n-1}^\delta + (F_n^{(1)} + F_n^{(2)}) r_{n-1}^\delta$.
2- Compute $r_n^\delta = y^\delta - Ax_n^\delta$.
3- If $\left\| r_n^\delta \right\| \leq \tau\delta$ *exit*
end

Theorem 4.2 *We assume that condition (4.3) is satisfied, then Algorithm 4.1 is stopped.*

Proof Because $\sup_{\lambda \geq 0} f_n(\lambda) = 1$for $n \geq 1$, then

$$\left\| (I - AA^* g_n(AA^*) \right\| = \left\| f_n(AA^*) \right\| \leq 1. \tag{4.4}$$

We observe that

$$\|r_{n^*-1}\|_Y \geq \left\| r_{n^*-1}^\delta \right\|_Y - \left\| (I - AA^* g_{n^*-1}(AA^*)) \left(y - y^\delta\right) \right\|_Y.$$

Since $\left\|r^{\delta}_{n^*-1}\right\|_Y > \tau\delta$ and by (4.4), we have

$$\|r_{n^*-1}\|_Y \geq \tau\delta - \delta = (\tau - 1)\delta.$$

Thus,

$$\left\|f_{n^*-1}(AA^*)y\right\|_Y \geq (\tau - 1)\delta.$$

Under the source condition (3.2) for $0 < s + 1/2 \leq n^* - 1$, then

$$\begin{aligned}
(\tau - 1)\delta &\leq \left\|f_{n^*-1}(AA^*)A(A^*A)^s u\right\|_Y \\
&= \left\|Af_{n^*-1}(A^*A)(A^*A)^s u\right\|_Y \\
&= \left\|(A^*A)^{1/2} f_{n^*-1}(A^*A)(A^*A)^s u\right\|_Y \\
&= \left\|\int_0^{\|A^*A\|} f_{n^*-1}(\lambda)\lambda^{s+1/2} dE_\lambda u\right\|_Y \\
&\leq \rho \sup_{\lambda\geq 0} \prod_{j=1}^{n^*-1} \frac{\alpha_j}{\alpha_j + \lambda} \sup_{\lambda\geq 0} \lambda^{s+1/2} \prod_{j=1}^{n^*-1} \frac{\alpha_j^2}{\alpha_j^2 + \lambda}.
\end{aligned}$$

By utilizing Lemma 3.1, we obtain

$$(\tau - 1)\delta \leq \rho c_s \gamma^{-(s+1/2)}_{n^*-1,2}.$$

where c_s with $0 < s \leq n^* - 3/2$ as in Theorem 3.1.

Therefore,

$$\gamma_{n^*-1,2} = \sum_{j=1}^{n^*-1} \alpha_j^{-2} \leq \widehat{c}_s \delta^{-2/(2s+1)}, \tag{4.5}$$

where $\widehat{c}_s = \left(\frac{\rho c_s}{(\tau-1)}\right)^{2/(2s+1)}$.

By considering $\alpha_j = q^j$, we can deduce that

$$\sum_{j=1}^{n^*-1} q^{-2j} \leq \widehat{c}_s \delta^{-2/(2s+1)}.$$

Thus,

$$n^* \leq \frac{\ln\left(\frac{1-q^2}{q^2}\widehat{c}_s \delta^{-2/(2s+1)} + \frac{1}{q^2}\right)}{2\ln\left(\frac{1}{q^2}\right)} < \infty.$$

This completes the proof. □

Now, by utilizing inequality (4.5) and considering condition (3.1), we have

$$\gamma_{n^*,2} \leq \left(\frac{1}{q} + 1\right)\gamma_{n^*-1,2} \leq \left(\frac{1}{q} + 1\right)\widehat{c}_s \delta^{-2/(2s+1)}.$$

Therefore,

$$\sqrt{\gamma_{n^*,2}}\delta \leq \widetilde{c}_s \delta^{2s/(2s+1)}, \tag{4.6}$$

where $\widetilde{c}_s = \sqrt{(1/q+1)\,\widehat{c}_s}$.

Lemma 4.3 *We assume that conditions (3.1) and (4.3) are satisfied. Under the source condition (3.2) with $0 < s \leq n^* - 3/2$, then*

$$\left\| x_{n^*}^{\delta} - x_{n^*} \right\|_X = O(\delta^{\frac{2s}{2s+1}}),$$

where n^* is defined by the discrepancy principle (1.4).

Proof : By Theorem 3.4 and (4.6), we have

$$\begin{aligned} \left\| x_{n^*}^{\delta} - x_{n^*} \right\|_X &\leq \sqrt{2\gamma_{n^*,2}}\delta \\ &\leq \sqrt{2}\widetilde{c}_s \delta^{2s/(2s+1)}. \end{aligned}$$

This completes the proof. □

Theorem 4.4 *We assume that conditions (3.1) and (4.3) are satisfied. Under the source condition (3.2) with $0 < s \leq n^* - 3/2$, then*

$$\left\| e_{n^*}^{\delta} \right\|_X = O(\delta^{\frac{2s}{2s+1}}),$$

where n^* is defined by the discrepancy principle (1.4).

Proof By (2.4), we have the representation

$$\begin{aligned} e_{n^*} &= \widehat{x} - g_{n^*}(A^*A)A^*y \\ &= \left(I - g_{n^*}(A^*A)A^*A\right)\widehat{x} \\ &= f_{n^*}(A^*A)\widehat{x}. \end{aligned}$$

Under the source condition (3.2), then

$$\begin{aligned} \|e_{n^*}\|_X &= \left\| f_{n^*}(A^*A)\left(A^*A\right)^s u \right\|_X \\ &= \left\| \left(A^*A\right)^s f_{n^*}(A^*A)u \right\|_X. \end{aligned}$$

By the interpolation inequality (see [1] p. 47, (2.49)), we get

$$\left\| \left(A^*A\right)^s f_{n^*}(A^*A)u \right\|_X \leq \left\| \left(A^*A\right)^{s+\frac{1}{2}} f_{n^*}(A^*A)u \right\|_X^{\frac{2s}{2s+1}} \left\| f_{n^*}(A^*A)u \right\|_X^{\frac{1}{2s+1}}.$$

Thus,

$$\|e_{n^*}\|_X \leq \left\| f_{n^*}(A^*A)u \right\|_X^{\frac{1}{2s+1}} \left\| \left(A^*A\right)^{\frac{1}{2}} f_{n^*}(A^*A)\left(A^*A\right)^s u \right\|_X^{\frac{2s}{2s+1}}$$

$$\leq \left\| f_{n^*}(A^*A) \right\|_X^{\frac{1}{2s+1}} \|u\|_X^{\frac{1}{2s+1}} \left\| \left(A^*A\right)^{\frac{1}{2}} f_{n^*}(A^*A) \left(A^*A\right)^s u \right\|_X^{\frac{2s}{2s+1}}$$

$$\leq \rho^{\frac{1}{2s+1}} \left\| \left(A^*A\right)^{\frac{1}{2}} f_{n^*}(A^*A) \left(A^*A\right)^s u \right\|_X^{\frac{2s}{2s+1}}. \tag{4.7}$$

Again, we have

$$\begin{aligned} \|r_{n^*}\|_Y &= \|Ae_{n^*}\|_X \\ &= \left\| Af_{n^*}(A^*A) \left(A^*A\right)^s u \right\|_X \\ &= \left\| \left(A^*A\right)^{\frac{1}{2}} f_{n^*}(A^*A) \left(A^*A\right)^s u \right\|_X . \end{aligned} \tag{4.8}$$

Now, substituting Eq. (4.8) in estimate (4.7), we obtain

$$\|e_{n^*}\|_X \leq \rho^{\frac{1}{2s+1}} \|r_{n^*}\|^{\frac{2s}{2s+1}}. \tag{4.9}$$

Further, we observe that

$$\begin{aligned} \|r_{n^*}\|_Y &= \left\| (I - AA^* g_{n^*}(AA^*) y \right\|_Y \\ &= \left\| (I - AA^* g_{n^*}(AA^*) \left(y - y^\delta\right) + y^\delta - AA^* g_{n^*}(AA^*) y^\delta \right\|_Y \\ &\leq \left\| (I - AA^* g_{n^*}(AA^*) \right\| \left\| y - y^\delta \right\|_Y + \left\| y^\delta - AA^* g_{n^*}(AA^*) y^\delta \right\|_Y . \end{aligned}$$

Through the relations (4.4), (1.2) and by the discrepancy principle (1.4), we derive

$$\|r_{n^*}\|_Y \leq \delta + \left\| r_{n^*}^\delta \right\|_Y \leq (1+\tau)\delta.$$

The inequality (4.9) implies that

$$\|e_{n^*}\|_X \leq \rho^{\frac{1}{2s+1}} (1+\tau)^{\frac{2s}{2s+1}} \delta^{\frac{2s}{2s+1}}.$$

Now, utilizing Lemma 4.3, we have the following result

$$\begin{aligned} \left\| e_{n^*}^\delta \right\|_X &\leq \|e_{n^*}\|_X + \left\| x_{n^*}^\delta - x_{n^*} \right\|_X \\ &\leq \left(\rho^{\frac{1}{2v+1}} (1+\tau)^{\frac{2s}{2s+1}} + \sqrt{2}\widetilde{c_s} \right) \delta^{\frac{2s}{2s+1}}. \end{aligned}$$

This completes the proof. □

5 Simulations

In this section, we present illustrative examples to demonstrate the effectiveness and validity of the proposed method. The results were obtained using MATLAB on a PC.

To assess the performance of our scheme relative to NSIT and MLI schemes, we conducted analyses using multiple test examples which correspond to integral equations of the first kind. The initial three examples represent one-dimensional synthesized problems, while the latter two examples pertain to the realm of two-dimensional image deblurring, which has emerged as one of the most formidable challenges.

Throughout all experiments, we calculate the solutions using both the NSIT method and the FNSIT method, employing the formulas (2.8) and (2.9) outlined in Example (2.1).

5.1 One-dimensional problems

The majority of problems in this collection involve discretizations of Fredholm integral equations of the first kind, which are typically characterized by severe ill-conditioning, we conducted analyses using multiple test examples sourced from Hansen's regularization tools (refer to [25] for more details). The formulation of the first-kind Fredholm integral equations can be expressed as:

$$\int_a^b k(s,t)f(t)dt = g(s),\ s \in [a,b]\,, \tag{5.1}$$

where $k(s,t) \in C([a,b]^2)$, $g \in L^2([a,b],\mathbb{R})$ are known functions and f is the unknown function to be determined in $L^2([a,b],\mathbb{R})$. The provided MATLAB package includes ill-conditioned matrices $\mathbf{A} \in \mathbb{R}^{N\times N}$, corresponding right-hand sides $\mathbf{b} \in \mathbb{R}^N$, and true solutions $\widehat{x} \in \mathbb{R}^N$ for these problems. The error-contaminated vector $\mathbf{b}^\delta$ is obtained as

$$\mathbf{b}^\delta = \mathbf{b} + \eta,$$

where $\eta = \varepsilon\,\|\mathbf{b}\|\text{randn}(\text{size}(\mathbf{b}))$ represents the error term and ε is the noise level.

During the experiments, we determine the regularization parameter n^* using the discrepancy principle (1.4) specified in Algorithm 4.1 where, $q = 0.75$ and $\tau = 1.01$.

For each example, we provide the average of the relative errors $\left\|\widehat{x} - x_{n^*}^\delta\right\|_2 / \|\widehat{x}\|_2$ (referred to as "RE") in the computed solution obtained using the FNSIT method discussed in Sect. 2, as well as the NSIT and MLI methods described in Sect. 1. These comparative evaluations are conducted for various combinations of N, ε, γ, and β.

Example 5.1 We consider the Fredholm integral equation of the first kind (5.1) with $k(s,t) = \exp(s \times cos(t))$, $g(s) = 2\sinh(s)/s$, and the interval $[a,b]$ defined as $[0,\pi]$. To discretize this integral equation, we employ a Galerkin method that utilizes orthonormal box functions as both test and trial functions. For this purpose, we utilize the Matlab program "*baart*". The resulting discretization yields a symmetric indefinite matrix $\mathbf{A}$, along with a scaled discrete approximation x that closely approximates the exact solution $f(t) = \sin(t)$.

Example 5.2 We consider the Fredholm integral equation (5.1) with

$$k(s,t) = \phi\,(t-s)\,,\ g(s) = (6-|s|)\left(1+\frac{1}{2}\cos\left(\frac{\pi s}{3}\right)\right) + \frac{9}{2\pi}\sin\left(\frac{\pi|s|}{3}\right),$$

where

$$\phi(t) = \begin{cases} 1 + \cos\left(\frac{\pi t}{3}\right), & |t| < 3, \\ 0, & |t| \geq 3, \end{cases}$$

and the interval $[a, b]$ defined as $[-6, 6]$.

To discretize this integral equation, we employ a Galerkin method that utilizes orthonormal box functions as both test and trial functions. For this purpose, we utilize the Matlab program "Phillips". The resulting discretization yields a symmetric indefinite matrix $\mathbf{A}$, along with a scaled discrete approximation x that closely approximates the exact solution $f(t) = \phi(t)$.

Example 5.3 We consider the Fredholm integral equation (5.1) in $[a, b] = [0, 1]$ with

$$k(s,t) = \begin{cases} s(t-1), & s < 0.5, \\ t(s-1), & s \geq 0.5, \end{cases} \quad \text{and} \quad g(s) = \begin{cases} \frac{4s^3-3s}{24}, & s < 0.5, \\ \frac{-4s^3+12s^2-9s+1}{24}, & s \geq 0.5. \end{cases}$$

To discretize the integral equation, we employ the Galerkin method with orthonormal box functions. The Matlab program "deriv2" from [25] is employed for this purpose.

Tables 1, 2, 3, 4 and 5 present a comprehensive analysis of the performance of our novel method in comparison to the NSIT and MLI methods. Upon careful examination,

Table 1 Displays the errors and number of iterations of the FNSIT method, NSIT method and MLI method for Examples 5.1–5.3 with $N = 2000$, $\beta = 0.8/\|A\|^{\gamma+1}$ and noise levels $\varepsilon = 0.1$

Method	Example 5.1		Example 5.2		Example 5.3	
	n^*	RE	n^*	RE	n^*	RE
FNSIT	4	0.32	2	0.028	11	0.11
NSIT	6	0.32	4	0.028	19	0.11
MLI ($\gamma = 0.5$)	39	0.33	12	0.068	4	0.11
MLI ($\gamma = 0.7$)	54	0.33	15	0.071	4	0.11
MLI ($\gamma = 0.9$)	69	0.33	22	0.070	5	0.11

Table 2 Displays the errors and number of iterations of the FNSIT method, NSIT method and MLI method for Examples 5.1–5.3 with $N = 2000$, $\beta = 0.8/\|A\|^{\gamma+1}$ and noise levels $\varepsilon = 0.01$

Method	Example 5.1		Example 5.2		Example 5.3	
	n^*	RE	n^*	RE	n^*	RE
FNSIT	10	0.17	3	0.021	18	0.033
NSIT	18	0.17	5	0.022	32	0.036
MLI ($\gamma = 0.5$)	696	0.17	57	0.023	82	0.036
MLI ($\gamma = 0.7$)	1490	0.17	84	0.023	131	0.037
MLI ($\gamma = 0.9$)	1885	0.17	120	0.023	83	0.037

Table 3 Displays the errors and number of iterations of the FNSIT method, NSIT method and MLI method for Examples 5.1–5.3 with $N = 2000$, $\beta = 0.8/\|A\|^{\gamma+1}$ and noise levels $\varepsilon = 0.005$

Method	Example 5.1		Example 5.2		Example 5.3	
	n^*	RE	n^*	RE	n^*	RE
FNSIT	11	0.15	3	0.019	19	0.024
NSIT	19	0.15	6	0.019	35	0.024
MLI ($\gamma = 0.5$)	965	0.15	75	0.020	133	0.027
MLI ($\gamma = 0.7$)	2067	0.15	110	0.020	244	0.028
MLI ($\gamma = 0.9$)	2613	0.15	157	0.020	155	0.028

Table 4 Displays the errors and number of iterations of the FNSIT method and NSIT method for Examples 5.1–5.3 with noise-free ($\varepsilon = 0$) and $N = 3000$

Method	Example 5.1		Example 5.2		Example 5.3	
	n^*	RE	n^*	RE	n^*	RE
FNSIT	56	0.029	40	4.24×10^{-6}	42	1.21×10^{-4}
NSIT	108	0.029	79	4.32×10^{-6}	84	1.31×10^{-4}

Table 5 Displays the errors and number of iterations of the FNSIT method and NSIT method for Examples 5.1–5.3 with noise-free ($\varepsilon = 0$) and $N = 4000$

Method	Example 5.1		Example 5.2		Example 5.3	
	n^*	RE	n^*	RE	n^*	RE
FNSIT	56	0.029	40	4.19×10^{-6}	42	1.20×10^{-4}
NSIT	108	0.029	80	4.27×10^{-6}	85	1.32×10^{-4}

two noteworthy observations emerge. Firstly, our method demonstrates clear superiority in terms of the number of iterations, consistently aligning with the relationship defined in Eq. (3.4). Secondly, our method showcases a high level of compatibility with other methods in terms of errors, and in certain instances, it even outperforms the NSIT and MLI methods.

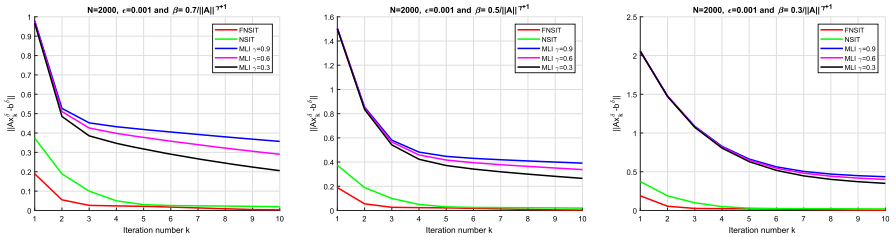

a) $\beta = 0.7/||A||^{\gamma+1}$. b) $\beta = 0.5/||A||^{\gamma+1}$. c) $\beta = 0.3/||A||^{\gamma+1}$.

Fig. 1 Test to compare the stopping iteration for Example 5.1 between the FNSIT method, the NSIT, and the MLI method with $N = 2000$, $\varepsilon = 0.001$, and different values of β

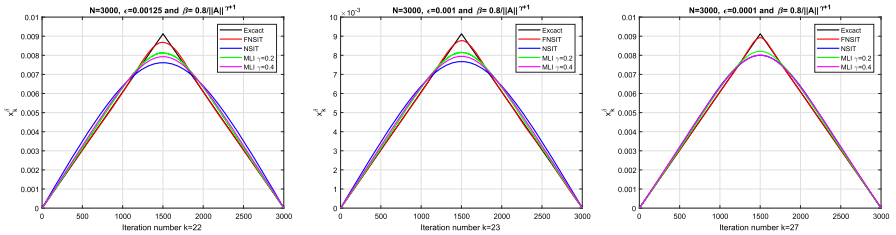

a) $k = 22$ and $\varepsilon = 0.00125$. b) $k = 23$ and $\varepsilon = 0.001$. c) $k = 27$ and $\varepsilon = 0.0001$.

Fig. 2 Example 5.3: The exact and approximate solutions at the k-th iteration by the FNSIT method, NSIT, and MLI method, with $N = 3000$, $\beta = 0.8/||A||^{\gamma+1}$ and varying values of ε

By examining Figs. 1 and 2, it becomes evident that our extensively conducted test comparing the stopping iteration for Example 5.3 across three distinct methods (FNSIT, NSIT, and MLI) reveals the superior performance of our studied method in terms of convergence. The number of iterations required by our method is significantly lower than that of NSIT and MLI, highlighting its efficiency and effectiveness.

5.2 Two-dimensional image deblurring

In this subsection, we provide two numerical examples to effectively demonstrate the performance of the FSNIT method in comparison to the NSIT method. Our primary focus lies in the application of space-invariant image deblurring. The blurring of images can be accurately modeled by employing a Fredholm integral equation of the first kind, expressed as

$$\int_{\Gamma} h(\widehat{s}, s, \widehat{t}, t) f(\widehat{s}, \widehat{t}) d\widehat{s} d\widehat{t} = g(s, t), \ (s, t) \in \Gamma, \tag{5.2}$$

where g represents the noisy blurred image, f signifies the original image, Γ is the domain of the exact image f and the function $h(\widehat{s}, s, \widehat{t}, t)$ pertains to the two-dimensional point spread function (PSF). In the case where the blur remains spatially invariant, meaning that it does not vary based on the spatial location, we observe that $h(\widehat{s}, s, \widehat{t}, t) = h(\widehat{s} - s, \widehat{t} - t)$. This particular characteristic holds true in the presented computational examples. Assuming that the images comprise $M \times N$ pixels, by discretizing the Fredholm integral equation (5.2), we encounter a problem in the form of equation $\mathbf{A}X = B$, where $\mathbf{A} \in \mathbb{R}^{NM \times NM}$ is the blurring matrix, $B \in \mathbb{R}^{NM}$ denotes the recorded blurred image and $X \in \mathbb{R}^{NM}$ represent the desired sharp image.

The PSF array for blurring in the computed examples can be characterized as a two-dimensional Gaussian function, and the elements of the unsealed PSF array are given by

$$P_{ij} = \exp\left(-0.5\left(\frac{i-k}{s}\right)^2 - 0.5\left(\frac{j-l}{s}\right)^2\right),$$

where the matrix P is the PSF array and (k, l) is the center of P.We assume the type of PSF is separable and the type of imposed boundary conditions is zero see, e.g., [26] for more details.

In general, the coefficient matrix $\mathbf{A}$ for separable blur has block structure of the form $\mathbf{A} = \mathbf{A}_r \otimes \mathbf{A}_c$ where $\mathbf{A}_c \in \mathbb{R}^{M\times M}$ and $\mathbf{A}_r \in \mathbb{R}^{N\times N}$. This special structure, and the symbol $\otimes$ that defines the operation that combines $\mathbf{A}_r$ and $\mathbf{A}_r$ in this way is called a Kronecker product.

Computing the singular value decomposition (SVD) of the matrix $\mathbf{A}$ is not trivial. To avoid this problem, we compute the SVD of the matrices $\mathbf{A}_r$ and $\mathbf{A}_c$, which is simple.

Using the basic properties of the Kronecker product, we get SVD of $\mathbf{A}$ by

$$\begin{aligned}\mathbf{A}_r \otimes \mathbf{A}_c &= \left(U_r \Sigma_r V_r^T\right) \otimes \left(U_c \Sigma_c V_c^T\right) \\ &= (U_r \otimes U_c)\,(\Sigma_r \otimes \Sigma_c)\,(V_r \otimes V_r)^T \\ &= U \Sigma V^T,\end{aligned}$$

where $[U_c, \Sigma_c, V_c]$ is the singular system of $\mathbf{A}_c$, $[U_r, \Sigma_r, V_r]$ is the singular system of $\mathbf{A}_r$ and $[U, \Sigma, V]$ is the singular system of the matrix $\mathbf{A}$.

To compute the blurred image B from the true image X, we use the formula

$$\mathbf{B} = \mathbf{A}_c \mathbf{X} \mathbf{A}_r,\ B = vect(\mathbf{B}) \in \mathbb{R}^{NM},$$

where $\mathbf{X} = reshape(X) \in \mathbb{R}^{NM\times NM}$.

The subsequent experiments serve to demonstrate the practical application of two-dimensional images that have undergone contamination due to both blur and Gaussian white noise, expressed as $B^\delta = B + \eta$, where $\eta = \varepsilon \|B\| randn(size(B))$ represents the error term and ε is the noise level.

In all experiments, the type of imposed boundary conditions is zero, and to quantify the quality of restoration, we employ the peak signal-to-noise ratio (PSNR), calculated using the formula

$$PSNR = 10 \log_{10} \left(\frac{NM}{\sum_{i=1}^{N} \sum_{i=1}^{M} \left(\mathbf{X}_{ij} - \mathbf{Y}_{ij}\right)^2} \right),$$

where $\mathbf{X}$ the original image and $\mathbf{Y}$ denotes the restored image.

Example 5.4 In our example, we consider the cameraman image, which is represented by an array of 248 × 248 pixels with noise level 1, 0.1 and 0.01%. In the test, we use the same iteration steps n for the FNSIT method and the NSIT method. This ensures that the computational cost remains consistent between the two methods. Our findings are presented in Figs. 3 and 4, and the performance of the peak signal-to-noise ratio is documented in Table 6.

(a) Exact image

(b) Blurred image with noise 1%

(c) Restored by FNSIT

(d) Restored by NSIT

Fig. 3 Image restored by 9 iterations with the FNSIT method (**c**) and NSIT method (**d**) where $\varepsilon = 1\%$

(a) Blurred image with noise 0.1%

(b) Restored by FNSIT

(c) Restored by NSIT

Fig. 4 Image restored by 14 iterations with the FNSIT method (**c**) and NSIT method (**d**) where $\varepsilon = 0.1\%$

Table 6 Behavior of PSNR under two cases by FNSIT method and NSIT method for Examples 5.4–5.5: 17 iterations with a noise level of 0.1% and 22 iterations with a noise level of 0.01%

Method	Example 5.4		Example 5.5	
	PSNR ($\varepsilon = 0.1\%$)	PSNR ($\varepsilon = 0.01\%$)	PSNR ($\varepsilon = 0.1\%$)	PSNR ($\varepsilon = 0.01\%$)
FNSIT	71.25	77.51	26.98	31.68
NSIT	65.92	67.88	23.87	25.83

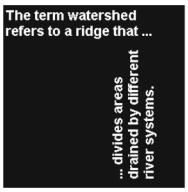

(a) Exact image

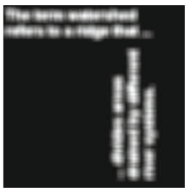

(b) Blurred image with noise 1%

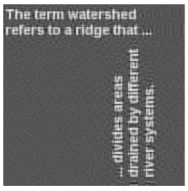

(c) Restored by FNSIT

(d) Restored by NSIT

Fig. 5 Image restored by 13 iterations with the FNSIT method (**c**) and NSIT method (**d**) where $\varepsilon = 1\%$

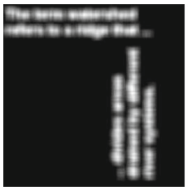

(a) Blurred image with noise 0.1%

(b) Restored by FNSIT

(c) Restored by NSIT

Fig. 6 Image restored by 19 iterations with the FNSIT method (**c**) and NSIT method (**d**) where $\varepsilon = 0.1\%$

Example 5.5 We consider the *text* image, which is represented by an array of 256×256 pixels with noise level 1, 0.1 and 0.01%. In the test, we use the same iteration steps n for FNSIT method and NSIT method. Our findings are presented in Figs. 5 and 6, and the performance of the peak signal-to-noise ratio is documented in Table 6.

The PSNR values presented in Table 6 demonstrate a notable improvement of our method compared to the NSIT method when considering the same number of iteration steps.

6 Conclusion

This article presents and examines a rapid iterative scheme designed to tackle and resolve ill-posed problems. Theoretical error estimates are substantiated through both

a-priori and a-posteriori regularization parameter strategies. The error bounds are demonstrated to be order optimal, particularly under the customary smoothness source conditions, with a focus on the bounded operator. Numerical examples effectively exhibit the validity of the theoretical findings, showcasing the advantages of the proposed method over the NSIT and MLI methods. Notably, our method outperforms the NSIT and MLI methods in terms of iteration requirements for achieving comparable accuracy.

While the NSIT scheme warrants additional numerical investigation, such research falls outside the scope of this study. However, there are several ideas for future exploration. For instance, one avenue worthy of exploration involves exploring the potential of substituting the current additional factor $F_n^{(2)}$ with a counterpart factor, aiming to achieve a reduced number of iterations while simultaneously enhancing error performance and rather to strive towards making each iteration more cost-effective.

Author Contributions The author have made substantial contributions to the work and are accountable for the integrity and accuracy of the content.

Funding None of the author received any financial support.

Data availability Data sharing is not applicable to this article as no datasets were generated or analyzed during the current study.

Declarations

Conflict of interest There are no potential conflict of interest.

Ethics approval Not applicable.

References

1. Engl, H.W., Hanke, M., Neubauer, A.: Regularization of Inverse Problems, vol. 375. Springer, Dordrecht (1996)
2. Lu, S., Pereverzev, S.V.: Regularization Theory for Ill-Posed Problems: Selected Topics, vol. 58. Walter de Gruyter, Berlin (2013)
3. Nair, M.T.: Linear Operator Equations: Approximation and Regularization. World Scientific, Singapore (2009)
4. Landweber, L.: An iteration formula for Fredholm integral equations of the first kind. Am. J. Math. **73**(3), 615–624 (1951)
5. Matysik, O., Van Hulle, M.M.: Simple-iteration method with alternating step size for solving operator equations in Hilbert space. J. Comput. Appl. Math. **300**, 290–299 (2016)
6. Neubauer, A.: On Nesterov acceleration for Landweber iteration of linear ill-posed problems. J. Inverse Ill-posed Probl. **25**(3), 381–390 (2017)
7. Xiong, X., Xue, X., Qian, Z.: A modified iterative regularization method for ill-posed problems. Appl. Numer. Math. **122**, 108–128 (2017)
8. Egger, H., Neubauer, A.: Preconditioning Landweber iteration in Hilbert scales. Numer. Math. **101**, 643–662 (2005)
9. Klann, E., Ramlau, R.: Regularization by fractional filter methods and data smoothing. Inverse Probl. **24**(2), 025018 (2008)
10. Hanke, M., Groetsch, C.W.: Nonstationary iterated Tikhonov regularization. J. Optim. Theory Appl. **98**, 37–53 (1998)

11. Huang, G., Reichel, L., Yin, F.: Projected nonstationary iterated Tikhonov regularization. BIT Numerical Mathematics **56**, 467–487 (2016)
12. Jin, Q., Zhong, M.: Nonstationary iterated Tikhonov regularization in Banach spaces with uniformly convex penalty terms. Numer. Math. **127**, 485–513 (2014)
13. Chang, W., D'Ascenzo, N., Xie, Q.: A relaxed iterated Tikhonov regularization for linear ill-posed inverse problems. J. Math. Anal. Appl. **530**(2), 127754 (2024)
14. Engl, H.W., Groetsch, C.W. (eds.): Inverse and Ill-posed Problems, vol. 4. Elsevier, Amsterdam (2014)
15. Kabanikhin, S.I.: Inverse and Ill-posed Problems: Theory and Applications. de Gruyter, Berlin (2011)
16. Gerth, D., Klann, E., Ramlau, R., Reichel, L.: On fractional Tikhonov regularization. J. Inverse Ill-posed Probl. **23**(6), 611–625 (2015)
17. Hochstenbach, M.E., Reichel, L.: Fractional Tikhonov regularization for linear discrete ill-posed problems. BIT Numer. Math. **51**, 197–215 (2011)
18. Jiang, M., Wang, G.: Convergence studies on iterative algorithms for image reconstruction. IEEE Trans. Med. Imaging **22**(5), 569–579 (2003)
19. Kaltenbacher, B., Neubauer, A., Scherzer, O.: Iterative Regularization Methods for Nonlinear Ill-posed Problems. Walter de Gruyter, Berlin (2008)
20. Hanke, M., Nagy, J., Plemmons, R.: Preconditioned iterative regularization for ill–posed problems (pp. 141–163). Institute for Mathematics and its Applications (USA) (1992)
21. Ceng, L.C., Ansari, Q.H., Wen, C.F.: Multi-step implicit iterative methods with regularization for minimization problems and fixed point problems. J. Inequal. Appl. **2013**, 1–26 (2013)
22. Van Hieu, D., Anh, P.K., Muu, L.D., Strodiot, J.J.: Iterative regularization methods with new stepsize rules for solving variational inclusions. J. Appl. Math. Comput. **68**, 571–599 (2022)
23. Han, G., Qu, G., Jiang, M.: Relaxation strategy for the Landweber method. Signal Process. **125**, 87–96 (2016)
24. Bechouat, T.: An implicit iteration method for solving linear ill-posed operator equations. Numer. Anal. Appl. **16**(2), 93–111 (2023)
25. Hansen, P.C.: Regularization tools version 4.0 for Matlab 7.3. Numer. Algorithms **46**, 189–194 (2007)
26. Hansen, P.C., Nagy, J.G., O'leary, D.P.: Deblurring Images: Matrices, Spectra, and Filtering. Society for Industrial and Applied Mathematics, Philadelphia (2006)